Nanoscale

PAPER

Cite this: *Nanoscale*, 2016, **8**, 12793

Highly transparent and flexible bio-based polyimide/TiO_2 and ZrO_2 hybrid films with tunable refractive index, Abbe number, and memory properties†

Tzu-Tien Huang,‡[a] Chia-Liang Tsai,‡[a] Seiji Tateyama,[b] Tatsuo Kaneko*[b] and Guey-Sheng Liou*[a]

Received 16th May 2016,
Accepted 5th June 2016

DOI: 10.1039/c6nr03963d

www.rsc.org/nanoscale

The novel bio-based polyimide (**4ATA-PI**) and the corresponding PI hybrids of TiO_2 or ZrO_2 with excellent optical properties and thermal stability have been prepared successfully. The highly transparent **4ATA-PI** containing carboxylic acid groups in the backbone could provide reaction sites for organic–inorganic bonding to obtain homogeneous hybrid films. These PI hybrid films showed a tunable refractive index (1.60–1.81 for **4ATA-PI/TiO_2** and 1.60–1.80 for **4ATA-PI/ZrO_2**), and the **4ATA-PI/ZrO_2** hybrid films revealed a higher optical transparency and Abbe's number than those of the **4ATA-PI/TiO_2** system due to a larger band gap of ZrO_2. By introducing TiO_2 and ZrO_2 as the electron acceptor into the **4ATA-PI** system, the hybrid materials have a lower LUMO energy level which could facilitate and stabilize the charge transfer complex. Therefore, memory devices derived from these PI hybrid films exhibited tunable memory properties from DRAM, SRAM, to WORM with a different TiO_2 or ZrO_2 content from 0 wt% to 50 wt% with a high ON/OFF ratio (10^8). In addition, the different energy levels of TiO_2 and ZrO_2 revealed specifically unique memory characteristics, implying the potential application of the prepared **4ATA-PI/TiO_2** and **4ATA-PI/ZrO_2** hybrid films in highly transparent memory devices.

Introduction

Recently, high refractive index polymer–inorganic hybrid materials have been widely advanced for their potential in optoelectronic applications.[1–3] Polymer–inorganic hybrid materials combine the advantages of organic polymers and inorganic materials which benefits the development of soft inorganic fabrication procedures. These materials have drawn great attention due to their outstanding properties such as refractive index, birefringence, Abbe's number, optical transparency, processability, and thermal stability when compared with the individual polymer or inorganic component.[4] For optical applications, the encapsulates for organic light-emitting diodes (OLEDs)[5] require materials with a high refractive index, low birefringence, high optical transparency, and a long-term ultraviolet light and thermal stability. Therefore, achieving a good combination of the above-mentioned properties is a crucial and ongoing issue.[6]

For the polymer matrix, great attention has been focused recently on the concept of sustainable development; thus, extensive scientific research development and efforts have been employed to prepare bio-based polymers for suppressing the use of fossil fuels without sacrificing performance. Many kinds of bio-based polymers have been developed to achieve a low-carbon society.[7] However, the glass transition temperature (T_g) of these polymers is too low for them to be used for industrial processes. In order to overcome this problem, high performance polyimides (PIs) with excellent thermal stability, high mechanical properties, good chemical and radiation resistance have been reported.[8] Moreover, introduction of alicyclic moieties could effectively lower the intra- and intermolecular charge transfer (CT) interactions of the PI chains to greatly enhance the transparency which is critical for optical applications.[9,10]

The inorganic materials most frequently reported in the literature concerning a high refractive index of organic–inorganic

[a]*Institute of Polymer Science and Engineering, National Taiwan University, Taipei, Taiwan 10617. E-mail: gsliou@ntu.edu.tw*

[b]*Research Area of Energy and Environment, Japan Advanced Institute of Science and Technology (JAIST), 1-1 Asahidai, Nomi, Ishikawa 923-1292, Japan. E-mail: kaneko@jaist.ac.jp*

†Electronic supplementary information (ESI) available: IR spectra, ^{1}H NMR spectra, thermal properties, UV-visible absorption spectra, cyclic voltammetry diagrams and retention times of these hybrid materials. See DOI: 10.1039/c6nr03963d

‡These authors contributed equally to this work.

This journal is © The Royal Society of Chemistry 2016

nanocomposites are TiO_2 (n = 2.7 at 500 nm in rutile form), ZrO_2 (n = 2.2 at 589 nm), ZnO (n = 2.0 at 550 nm), CeO_2 (n = 2.18 at 500 nm) and ZnS (n = 2.4 at 500 nm). These high refractive index inorganic materials are used as nanoscale building blocks because they are highly available; TiO_2 and ZrO_2 are widely applied as UV-shielding pigments in the field of optical research and the polymer industry.[11] In previous studies,[12,13] the refractive index of the polymer/titania hybrids increases with increasing the TiO_2 content, but the transparency is reduced dramatically at a 400 nm wavelength, attributed to the low band gap of TiO_2 (3.2 eV), resulting in a pale yellow color of the obtained hybrid films. Meanwhile, the polymer/zirconia hybrid films exhibited higher transparency in the visible light region due to the larger energy band gap of ZrO_2 (5.0–5.85 eV) than that of the corresponding polymer/titania system.[12,13] Thus, choosing species of inorganic materials in the hybrid system is an important issue for enhancing the refractive index without sacrificing optical transparency in the visible light region. Furthermore, the domain size of inorganic materials must be well controlled within only 5 nm for lowering scattering loss and retaining the optical transparency in optical applications.[14] Chemical reaction based on the *in situ* sol–gel hybridization approach is a facile method to overcome the agglomeration problem of nanoparticles by manipulating the organic/inorganic interfacial interactions at various molecular and nanometer length scales.[12]

Recently, polymer hybrids have also drawn a lot of attention in memory device applications. CT complex formation could be further enhanced by introduction of supplementary components into the polymer hybrid such as electron donors or electron acceptors.[15] Inorganic materials with a strong electron-withdrawing capability due to the lower LUMO energy level could enhance the CT effect, thus interesting memory behavior should be expected. As compared with the polymer memory devices with organic molecules or metallic particles, relatively few studies have been conducted on polymer memory devices containing semiconducting particles.[16] The introduction of TiO_2 or ZrO_2 could prevent the detriment of decreasing the ON/OFF ratios at a high TiO_2 or ZrO_2 content because of the low conductivity in the OFF state.[12d,f] The operating mechanism of the polymer hybrids can be attributed to charge transfer for memory applications, and the thickness is always controlled within 100 nm. Thus, the domain size of the inorganic particles dispersed in the polymer matrix is the key issue for nanoscale memory devices.

Herein, a new bio-based polyimide **4ATA-PI** was synthesized from the bio-based alicyclic diamine, 4,4′-diamino-α-truxilic acid (4ATA), and alicyclic dianhydride (BCDA) in this study. The carboxylic acid groups in the PI chains could provide the organic–inorganic bonding sites to obtain highly transparent and flexible bio-based polyimide/TiO_2 and ZrO_2 hybrid films; then, the optical properties (such as transparency, refractive index, and Abbe number) and memory behavior are investigated.

Experimental

Materials

4,4′-Diamino-α-truxillic acid dihydrochloride (**4ATA-salt**) was synthesized according to the previous literature.[17] Commercially available alicyclic dianhydride bicyclo[2.2.2]-oct-7-ene-2,3,5,6-tetracarboxylic dianhydride (BCDA) (Mp: 300 °C, from ITRI) was purified by vacuum sublimation. *N*,*N*-Dimethylacetamide (DMAc) (TEDIA), triethylamine (TEA) (Across) and gamma-butyrolcetone (GBL) (Across) and other reagents were used as received from commercial sources.

Preparation of 4ATA-PI

The **4ATA-salt** (0.399 g, 1.00 mmol) and 1.5 mL DMAc were added into a two-necked 50 mL glass reactor under nitrogen. The reaction mixture was heated at 110 °C for 30 min to dissolve the **4ATA-salt** and 0.556 mL TEA was added into the reactor to produce the **4ATA-diamine-salt**. Then, BCDA (0.248 g, 1.00 mmol) and 1.5 mL GBL were added, and the polymerization was carried out at room temperature for 24 h. The poly(amic acid) precursor could be dehydrated to the polyimide by treatment with isoquinoline at 170–180 °C for 15 h. The obtained polymer solution was poured slowly into 300 mL methanol and the water co-solvent. Finally, the **4ATA-PI-salt** was dissolved in DMAc and 0.07 mL HCl was added to yield **4ATA-PI** which was poured slowly into 300 mL methanol and water co-solvent and dried under reduced pressure at 120 °C for 6 hours (Scheme 1). The inherent viscosity, average molecular weight, and solubility behavior of the obtained polyimide **4ATA-PI** are summarized in Table 1.

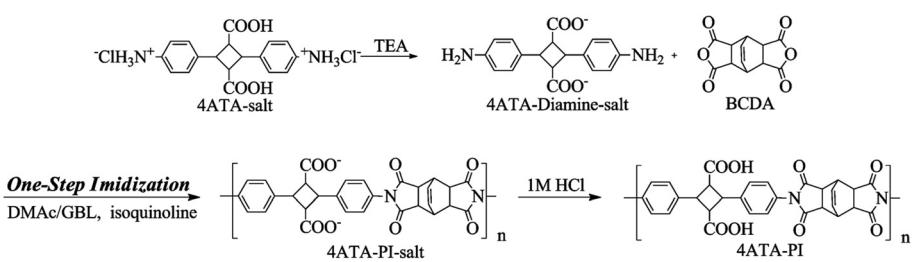

Scheme 1 Synthesis of the bio-based polyimide **4ATA-PI**.

 This journal is © The Royal Society of Chemistry 2016

Table 1 Inherent viscosity, GPC data, and solubility behavior of **4ATA-PI**

		GPC data[b]			Solubility in various solvents[d]						
Polymer	η^a (dL g^{-1})	M_n	M_w	PDI[c]	NMP	DMAc	DMF	DMSO	*m*-Cresol	THF	$CHCl_3$
4ATA-PI	0.70	25 600	34 200	1.34	++	++	++	++	++	–	–

[a] Measured at a polymer concentration of 0.5 g dL^{-1} in DMAc at 30 °C. [b] Calibrated with polystyrene standards, using NMP as the eluent at a constant flow rate of 0.5 mL min^{-1} at 40 °C. [c] Polydispersity index (M_w/M_n). [d] The solubility was determined using 2 mg sample in 2 mL of solvent. ++: soluble at room temperature, +: soluble on heating, ±: partially soluble or swelling on heating, –: insoluble even on heating.

Preparation of the 4ATA-PI films

The solution of **4ATA-PI** in DMAc was casted onto glass substrates and dried at 80 °C for 6 h, and at 150 °C for 8 h under vacuum. Finally, the **4ATA-PI** film with a thicknesses of 20 μm could be obtained and used for solubility tests, and optical and thermal measurements.

Preparation of the 4ATA-PI/titania and 4ATA-PI/zirconia hybrid films

The synthesis of **4ATA-PITi50** was used as an example to illustrate the general synthesis route used to produce the hybrid films of **4ATA-PITiX** (Scheme 2). Firstly, 0.05 g of **4ATA-PI** was dissolved in 3 mL of DMAc, and 0.1 mL of HCl was added very slowly into the PI solution and further stirred at room temperature for 30 min. Then, 0.152 mL (0.45 mmol) of $Ti(OBu)_4$ dissolved in 0.152 mL of butanol was added drop-wise into the above solution by a syringe, and then stirred at room temperature for 2 hours. Finally, the resulting precursor solution was filtered through a 0.45 mm PTFE filter and drop-coated onto glass substrates. The preparation of the **4ATA-PI/zirconia** (**4ATA-PIZrX**) hybrid is similar to that of **4ATA-PI/titania** mentioned above, and **4ATA-PIZr50** was used as an example to illustrate the procedure for producing the hybrid **4ATA-PIZrX** (Scheme 2). Firstly, 0.05 g of **4ATA-PI** was dissolved in 3 mL of DMAc, and then 0.10 mL of acetic acid was added very slowly into the PI solution and further stirred at room temperature for 30 min. Then, 0.21 mL (0.62 mmol) of $Zr(OBu)_4$ dissolved in 0.21 mL of butanol was added drop-wise into the above solution by a syringe, and then stirred at room temperature for 10 min. Finally, the resulting precursor solution was filtered through a 0.45 mm PTFE filter and drop-coated onto glass substrates.

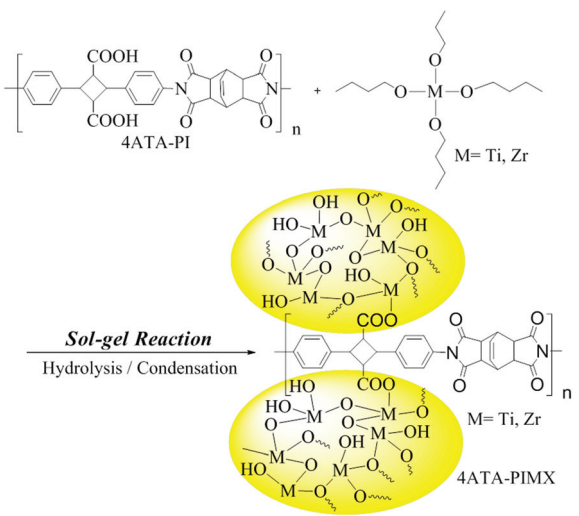

Scheme 2 Synthesis and structures of the **4ATA-PI/TiO_2** and **4ATA-PI/ZrO_2** hybrids.

For the preparation of optical hybrid films with a thickness of about 20 ± 3 μm, the above precursor solution was cast onto a glass plate followed by a subsequent heating program at 60 °C for 4 h, 150 °C for 2 h, and then 300 °C for 2 h under vacuum. In addition, the above-prepared solution was also spin-coated onto a glass plate or silicon wafer at 1000–2500 rpm for 1 min. The obtained film was then treated by a heating process of 80, 150, and 250 °C for 30 min, and 300 °C for 60 min, respectively, to afford hybrid thin films with thicknesses of 500–600 nm. The flexible, transparent, and homogeneous **4ATA-PIMX** hybrid optical films with a different titania or zirconia content could be successfully prepared.

Measurements

Fourier transform infrared (FT-IR) spectra were recorded on a PerkinElmer Spectrum 100 Model FT-IR spectrometer with a resolution of 1 cm^{-1} and a number of scans of 4. ^{1}H NMR spectra were measured on a Bruker AV 500 MHz spectrometer in DMSO-d_6, using tetramethylsilane as an internal reference. The inherent viscosities were determined at 0.5 g dL^{-1} concentration using a Tamson TV-2000 viscometer at 30 °C. Thermogravimetric analysis (TGA) conducted with TA Instruments Q50 and experiments were carried out on approximately 3–5 mg film samples heated in flowing nitrogen or air (flow rate: 20 cm^3 min^{-1}) at a heating rate of 20 °C min^{-1}. The coefficient of thermal expansion (CTE) and glass transition temperatures (T_g) were measured by a dilatometer (TA instrument SI-5 TMA Q400EM). The TMA experiments were conducted from 40 to 450 °C at a scan rate of 10 °C min^{-1} by a tensile probe under an applied constant load of 50 mN. T_g was taken as the onset temperature of probe displacement on the TMA traces, and the CTE data were determined in the range of 40–300 °C. Ultraviolet-visible (UV-vis) spectra of the obtained films were recorded on a Hitachi U-4100 UV-vis-NIR spectrophotometer. An ellipsometer (SOPRA, GES-5E) was used to measure the refractive index (n) of the prepared films in the wavelength range of 300–800 nm, and the thickness (h) was also deter-

mined simultaneously. The in-plane (n_{TE}) and out-of-plane (n_{TM}) refractive indices of the films formed on the silica substrates were measured using a prism coupler (Metricon, PC-2000) at wavelengths of 632.8 nm at room temperature. The in-plane/out-of-plane birefringence (Δn) was calculated as $\Delta n = n_{TE} - n_{TM}$. The microstructure of the prepared PI hybrid films was examined using JOEL JEM-1230 transmission electron microscopy (TEM) at an operating voltage of 100 kV. Cyclic voltammetry (CV) was performed with a Bioanalytical System Model CV-27 and conducted with the use of a three-electrode cell in which ITO (polymer film area of about 0.5 × 1.2 cm^2) was used as the working electrode and a platinum wire as the auxiliary electrode at a scan rate of 100 mV s^{-1} against a Ag/AgCl reference electrode in anhydrous CH_3CN, using 0.1 M of TBAP as the supporting electrolyte. All cell potentials were taken using a home-made Ag/AgCl KCl (sat.) reference electrode.

Fabrication and measurement of the memory devices

The memory devices were fabricated with the configuration of ITO/thin film/Al. The ITO glass used for the memory devices was cleaned by ultrasonication with water, acetone, and isopropanol each for 30 min. The hybrid thin films were prepared according to the previous procedure using ITO as a substrate, and the film thickness was adjusted to be around 50 nm. Finally, a 300 nm thick Al top electrode was thermally evaporated through the shadow mask (recorded device units of 0.5 × 0.5 mm^2 in size) at a pressure of 10^{-7} Torr with a depositing rate of 3–5 Å s^{-1}. The electrical characterization of the memory device was performed using a Keithley 4200-SCS semiconductor parameter analyzer equipped with a Keithely 4205-PG2 arbitrary waveform pulse generator. ITO was used as the cathode (maintained as common), and Al was set as the anode during the voltage sweep. The probe tip used 10 mm diameter tungsten wire attached to a tinned copper shaft with a point radius <0.1 mm (GGB Industries, Inc.).

Molecular simulation

Molecular simulation in this study was carried out with the Gaussian 09 program package. The equilibrium ground state geometry and electronic properties of the basic unit in the polyimide were optimized by means of the density functional theory (DFT) method at the B3LYP level of theory (Beckesstyle three-parameter density functional theory using the Lee–Yang–Parr correlation functional) with the 6-31G(d) basis set.

Results and discussion

Polymer synthesis and characterization

New **4ATA-PI** was prepared by **4ATA-diamine-salt** with BCDA in DMAc and the GBL co-solvent system to form the precursor poly(amic acid), and could be dehydrated to the polyimide by treatment with isoquinoline at 170–180 °C for 15 h, and then using HCl to transform **4ATA-PI-salt** to **4ATA-PI** (Scheme 1). Finally, **4ATA-PI** precipitated in white fiber-like forms when slowly pouring the resulting PI solution into methanol and water co-solvent. The **4ATA-diamine-salt** used in this study was synthesized by the material which was extracted from *E. coli* and prepared by [2 + 2] photo-cycloaddition.[17] This bio-based alicyclic diamine is good for a sustainable low-carbon society; in addition, PI derived from this alicyclic diamine with alicyclic dianhydride could lower charge transfer (CT) interactions to enhance the transparency of the obtained PI. The inherent viscosity, molecular weight, and solubility behavior of the obtained **4ATA-PI** are summarized in Table 1. **4ATA-PI** was soluble in polar aprotic organic solvents such as NMP, DMAc, DMF, and DMSO and could be solvent-cast into a flexible and transparent polymer film as shown in Fig. 1a. The FT-IR spectrum of the **4ATA-PI** film shown in Fig. S1 (ESI†) exhibits an absorption band in the region of 2500 to 3300 cm^{-1} (carboxylic acid O–H stretch) and characteristic imide absorption bands at 1775 cm^{-1} (asymmetrical C═O), 1725 cm^{-1} (symmetrical C═O), 1370 cm^{-1} (C–N), and 734 cm^{-1} (imide ring deformation). Yield: 86.4%. The ^{1}H NMR (500 MHz, DMSO-d_6, δ, ppm) spectrum was also measured and is depicted in Fig. S2 (ESI†). Thus, a novel bio-based PI was successfully synthesized and fabricated into a film by the solution-casting processes for practical applications.

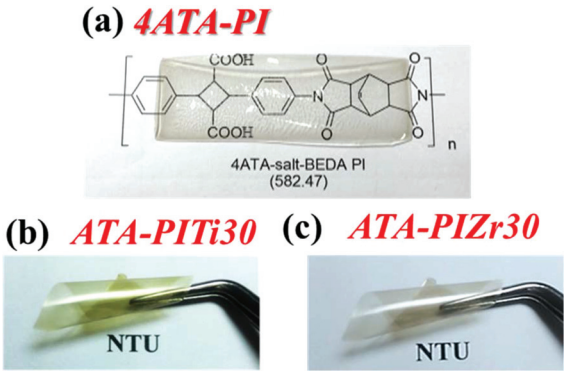

Fig. 1 Flexible and transparent (a) **4ATA-PI**, (b) **4ATA-PITi30** and (c) **4ATA-PIZr30** optical films (thickness: 30 ± 5 μm).

Synthesis and characterization of PI hybrids

The procedure of the **4ATA-PI/titania** and **4ATA-PI/zirconia** hybrid (**4ATA-PIMX**) films prepared by the sol–gel reaction of **4ATA-PI** with titania or zirconia precursors is depicted in Scheme 2, and the reaction compositions are also summarized in Table 2. The carboxylic acid groups in the backbone of **4ATA-PI** could provide reaction sites for organic–inorganic bonding, resulting in the homogeneous, flexible, and transparent hybrid films as shown in Fig. 1. The FT-IR spectra of the **4ATA-PITi30** and **4ATA-PIZr30** hybrid films shown in Fig. S3 (ESI†) exhibit broad absorption bands in the region of 3000 to 3700 cm^{-1} (O–H stretch). The signal strength is stronger than that for **4ATA-PI** due to the hydroxyl groups of the titania and zirconia. In addition, the inorganic Ti–O–Ti and Zr–O–Zr band could also be observed at 650–800 and 600–650 cm^{-1}, which is also similar to that in the previous report.[12,13]

This journal is © The Royal Society of Chemistry 2016

Table 2 Thermal properties of **4ATA-PI** hybrid films with TiO_2 and ZrO_2

Index	T_g [a] (°C)	α before T_g [b] (μm m^{-1} °C)	Reactant composition (wt%)		Hybrid film inorganic content (wt%)		T_d^5 [d] (°C)		T_d^{10} [d] (°C)		R_{w800} [e] (%)
			4ATA-PI	$Ti(OBu)_4/Zr(OBu)_4$	Theoretical	Experimental[c]	N_2	Air	N_2	Air	
4ATA-PI	369	56	100	0	0	0	395	390	410	410	23.0
4ATA-PITi10	385	45	67.8	32.2	10	9.9	385	395	415	415	33.7
4ATA-PITi30	415	34	35.4	64.6	30	28.4	390	400	420	420	63.0
4ATA-PITi50	—	—	19.0	81.0	50	48.5	400	405	450	435	70.6
4ATA-PIZr10	387	43	74.3	25.7	10	10.9	385	350	405	380	37.5
4ATA-PIZr30	410	30	42.8	57.2	30	29.4	390	395	415	400	62.8
4ATA-PIZr50	—	—	24.3	75.7	50	49.2	400	400	450	415	70.3

[a] Glass transition temperature measured by TMA with a constant applied load of 5 mN at a heating rate of 10 °C min^{-1} by tension mode. [b] The CTE data were determined over a 50–200 °C range by tension mode. [c] Experimental inorganic content estimated from TGA curves. [d] Temperature at which 5% and 10% weight loss occurred, respectively, recorded by TGA at a heating rate of 20 °C min^{-1} and a gas flow rate of 30 cm^3 min^{-1}. [e] Residual weight percentages at 800 °C under nitrogen flow.

Thermal properties of 4ATA-PI, 4ATA-PI/TiO_2 and 4ATA-PI/ZrO_2

The thermal properties of the bio-based **4ATA-PI**, **4ATA-PI/TiO_2** and **4ATA-PI/ZrO_2** hybrid films (**4ATA-PIMX**) were investigated by TGA and TMA, and the results are listed in Table 2. The resulting PI hybrid materials revealed high thermal stability by TGA measurement both in nitrogen and air, and the char yield increased with the increasing inorganic materials content as shown in Fig. S6 (ESI†). In addition, the inorganic content in the hybrid materials could be confirmed by the char yields under air flow, and were in good agreement with the theoretical values, which also ensured successful incorporation of these inorganic nanoparticles.

The TMA thermal analysis of **4ATA-PI** exhibited T_g up to 369 °C, which may be due to hydrogen bonding between the carboxylic acid groups that enhances the intermolecular forces. Furthermore, T_g of the PI hybrids increased with the increasing inorganic content.

For the titania system, T_g increased to 415 °C with 30 wt% TiO_2 content, and T_g increased to 410 °C with 30 wt% ZrO_2 content for the zirconia system as shown in Fig. S7 (ESI†). In addition, the coefficient of thermal expansion (CTE) is an important reference parameter for polymer films in microelectronic applications, and the CTE of the **4ATA-PI** and **4ATA-PI** hybrid films is also summarized in Table 2. Generally, inorganic reinforced components often reveal a much lower CTE value than that of organic matrixes, which suppress the CTE of the resulting hybrid materials. Therefore, the CTE of these PI hybrids decreased with increasing the volume fraction of inorganic nanoparticles.

Optical properties of the optical polymer and hybrid films

The UV-vis transmission spectra of the **4ATA-PI**, **4ATA-PI/TiO_2** and **4ATA-PI/ZrO_2** hybrid thick (thickness: 20 ± 3 μm) and thin (thickness: 500–600 nm) films were measured, and the results are summarized in Fig. 2 and Table 3. The **4ATA-PI** film derived from alicyclic dianhydride was optically colorless due to the lower intra- and intermolecular charge transfer (CT) interactions. Therefore, the transparency of the **4ATA-PI** thin film could reach 94% at 400 nm. However, the optical transparency of the corresponding **4ATA-PI/TiO_2** hybrid films reduced dramatically at 400 nm, attributed to the low band gap of TiO_2 (3.2 eV), resulting in pale yellow hybrid films even though the domain size of titania is less than 10 nm, and the red-shift phenomenon could also be ascribed to the slight variation in the particle size with an increase of the inorganic amount in the hybrid film.[12] On the contrary, the **4ATA-PI/ZrO_2** hybrid films could maintain a higher transparency in the visible light region due to a larger energy band gap of ZrO_2 (5.0–5.85 eV) than that of the corresponding **4ATA-PI/TiO_2** system. These **4ATA-PI/ZrO_2** hybrid films with a well-dispersed zirconia domain size of less than 10 nm as shown in Fig. 3 revealed excellent optical transparency with lower cut-off wavelengths in the UV region. The refractive index dispersion in the range of 300–800 nm is depicted in Fig. 4, and the inset figure shows the variation of refractive index at 633 nm with a different titania and zirconia content. The refractive index increased with increasing the inorganic content, indicating that the sol–gel reaction between **4ATA-PI** and the Ti–OH or Zr–OH groups of the inorganic precursors formed the Ti–O–Ti and Zr–O–Zr structures, which promoted the refractive index effectively. In addition, the Abbe number (V_d, variation of refractive index *versus* wavelength) also is an important parameter for optical materials, with high values of V_d indicating low dispersion. Interestingly, the **4ATA-PI/ZrO_2** hybrid system not only could increase the refractive index greatly but also enhance Abbe's number much more effectively than the corresponding TiO_2 hybrid system. Thus, the **4ATA-PI/ZrO_2** hybrid optical films with a tunable refractive index effect, higher transparency and Abbe number than those of the **4ATA-PI/TiO_2** hybrid films demonstrate the advanced values for optical applications.

Memory device characteristics and switching mechanism

The UV-vis absorption spectra of **4ATA-PI** are depicted in Fig. S8 (ESI†), and the onset wavelength of optical absorption was utilized to obtain the optical energy band gap (E_g). The electrochemical properties of **4ATA-PI** were investigated by cyclic voltammetry (CV) using 0.1 M tetrabutyl ammonium

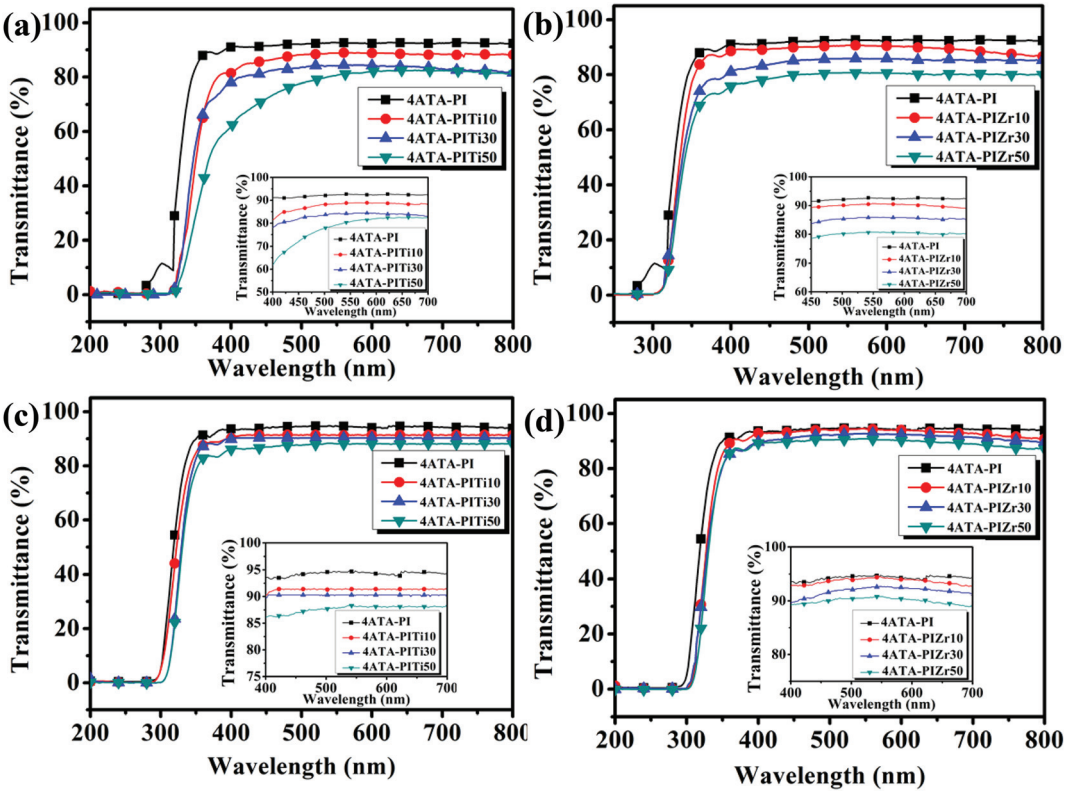

Fig. 2 Optical transmission spectra of **4ATA-PITiX** and **4ATA-PIZrX** thick hybrid films (a) and (b) (thickness: 20 ± 5 μm), and thin films (c) and (d) (thickness: 500–600 nm). The inset figures show the transmission spectra of the hybrid thick and thin films at a 450–700 nm wavelength.

Table 3 Optical properties of the **4ATA-PI** hybrid films

	λ_0 [a] (nm)	T_{400} [b] (%)	T_{450} [b] (%)	n [c]	Δn [d]	V_d [e]
4ATA-PI	320/280	91/94	92/93	1.598	0.0068	25.72
4ATA-PITi10	325/300	82/91	86/91	1.669	0.0079	25.00
4ATA-PITi30	326/307	78/89	82/90	1.734	0.0098	24.73
4ATA-PITi50	329/310	62/86	72/87	1.807	0.0112	26.30
4ATA-PIZr10	322/298	89/93	90/92	1.658	0.0074	33.15
4ATA-PIZr30	324/300	81/90	84/91	1.725	0.0094	34.76
4ATA-PIZr50	326/301	76/89	79/90	1.795	0.0109	36.31

[a] The cut-off wavelength (λ_0) from the UV-vis transmission spectra of polymer thick films/thin films (thickness: 20 ± 3 μm/500–600 nm). [b] Transmittance of polymer thick films/thin films (thickness: 20 ± 3 μm/500–600 nm) at 400 nm and 450 nm. [c] Refractive index at 633 nm by ellipsometer. [d] The in-plane/out-of-plane birefringence (Δn) calculates as $\Delta n = n_{TE} - n_{TM}$ using a prism coupler. [e] Abbe's number is given by $V_d = n_{587.56} - 1/n_{486.1} - n_{656.3}$.

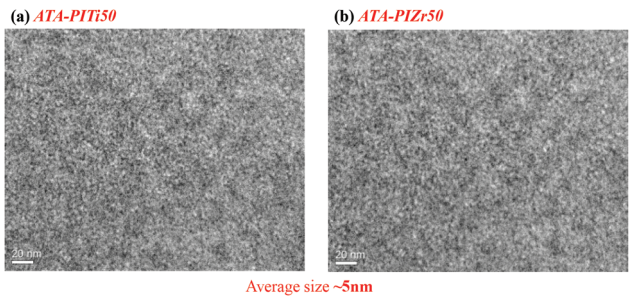

Fig. 3 TEM images of (a) **4ATA-PITi50** and (b) **4ATA-PIZr50** hybrid materials.

perchlorate (TBAP) as the supporting electrolyte under nitrogen atmosphere. The typical CV diagram of **4ATA-PI** is depicted in Fig. S9 (ESI†), and the onset oxidation was used to calculate the HOMO energy level. The redox potential of **4ATA-PI** and the respective HOMO and LUMO energy values are estimated and summarized in Table 4.

The memory behavior of **4ATA-PI** was depicted by the current–voltage (*I–V*) curves of an ITO/polymer/Al sandwich device as shown in Scheme 3, and Al was used as the electrode for applying voltage during the sweep. The polymer film thickness was optimized to around 50 nm because of the thickness effect of the polymer film on memory behavior reported previously.[18]

Fig. 5 reveals the *I–V* curves of **4ATA-PI**, and the device could not be switched to the ON state, and only stayed in the OFF state with a current range of 10^{-13} to 10^{-15} A both in the positive and negative sweeps up to 6 V and −6 V, respectively, indicating non-memory characteristics.

In order to get more insight into the **4ATA-PI** memory behaviour, a molecular simulation of the basic unit was carried out by DFT/B3LYP/6-31G(d) with the Gaussian 09 program. The HOMO and LUMO energy levels calculated by molecular

 This journal is © The Royal Society of Chemistry 2016

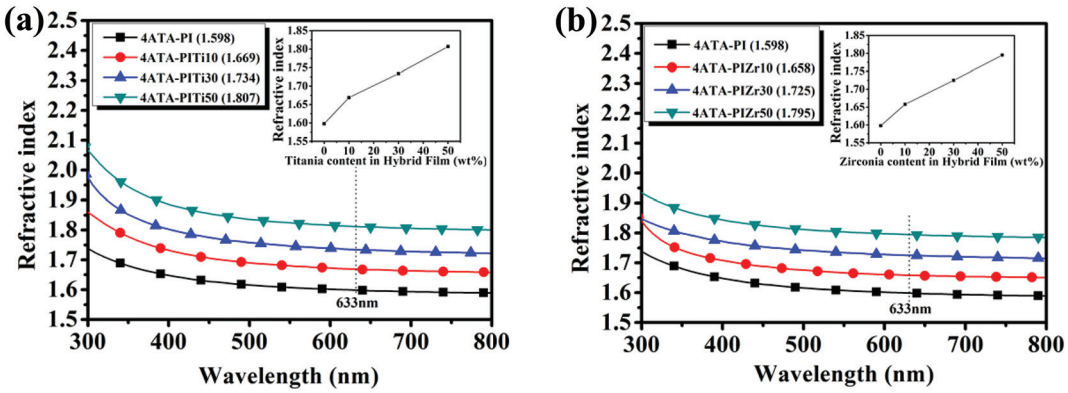

Fig. 4 Variation of the refractive index for the (a) **4ATA-PITiX** and (b) **4ATA-PIZrX** hybrid films with wavelength. The inset figures show the refractive index at 633 nm with a different titania and zirconia content.

Table 4 Redox potential and energy level of **4ATA-PI**

Polymer	UV-vis absorption (nm) λ_{onset}	Oxidation potential[a] (V) E_{onset}	E_g[b] (eV)	HOMO[c] (eV)	LUMO (eV)
4ATA-PI	359	0.96	3.45	−5.40	−1.95

[a] The data compared with Ag/AgCl in CH_3CN. [b] The data were calculated from polymer films by the equation: $E_g = 1240/\lambda_{onset}$ (energy gap between HOMO and LUMO). [c] The HOMO energy levels were calculated from CV and were referenced to ferrocene (4.8 eV, onset = 0.36 V)

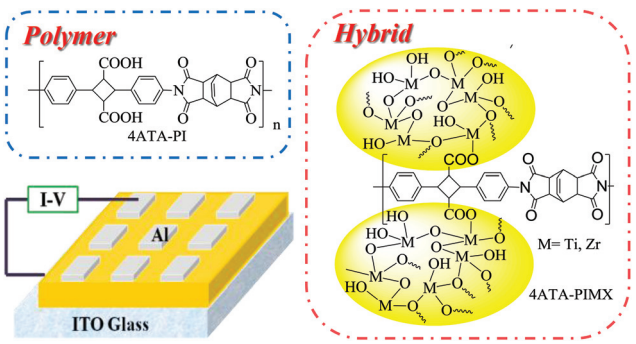

Scheme 3 Chemical structures of **4ATA-PI**, **4ATA-PI/TiO_2**, and **4ATA-PI/ZrO_2**, and the schematic diagram of the memory device consisting of a polymer thin film sandwiched between ITO bottom and Al top electrodes.

simulation were in agreement with the experimental values, and the charge density isosurfaces of the basic unit are summarized in Fig. 6. According to a previous report,[19] when the applied electric field reaches the switching-on voltage, some electrons at the HOMO accumulate energy and transit to the LUMO, forming a charge transfer complex (ON state) by different ways. The memory device of **4ATA-PI** exhibited non-memory characteristics because **4ATA-PI** is without obvious electron-donating and electron-withdrawing groups; besides, the energy band gap is too high to stabilize the electron in the LUMO. Thus, CT could not occur through several courses to form the conductive CT complexes as shown in Fig. 9a.

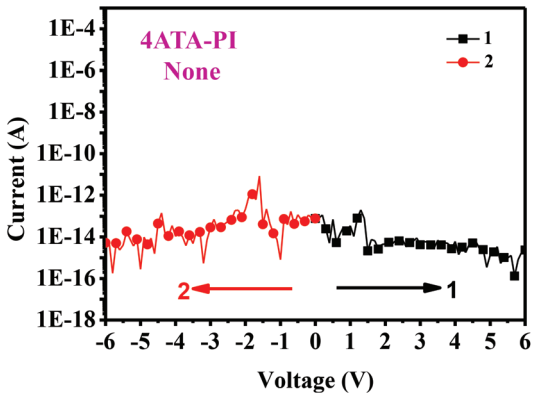

Fig. 5 Current–voltage (I–V) characteristics of the ITO/**4ATA-PI** (50 ± 3 nm)/Al memory device.

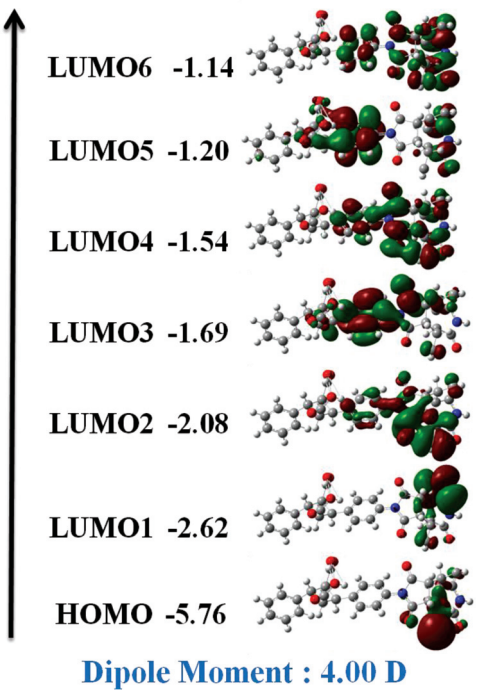

Fig. 6 Calculated molecular orbitals and corresponding energy levels of the basic units for **4ATA-PI**.

In addition, the *I–V* curves of memory devices derived from the PI hybrids with TiO_2 and ZrO_2 as electron acceptors are shown in Fig. 7 and 8, respectively.

Fig. 7a and b are the *I–V* curves of the **4ATA-PITi5** hybrid with 5 wt% of TiO_2. The devices based on **4ATA-PITi5** could not be switched to the ON state, maintaining the OFF state with a current range of 10^{-13} to 10^{-15} A in the positive sweep up to 6 V. However, a sharp increase in the current could be observed at −4.7 V at about 50% during the negative sweep, meaning that the device undergoes an electrical transition from the OFF state to the ON state (writing process). The device could remain in the ON state during the subsequent negative (the third sweep) and positive (the fourth sweep) scans. Thus, the **4ATA-PITi5** memory device could not be reset to the initial OFF state by applying a reverse electric field, indicating non-erasable behaviour. The fifth sweep was conducted after turning off the power for about 15 s, and it was found that the ON state had relaxed to the original OFF state without an erasing process, and then the device could be switched to the ON state again at the threshold voltage of −3.9 V. Thus, the device behaves with a short retention time and re-writable property which are indicative of DRAM characteristics.

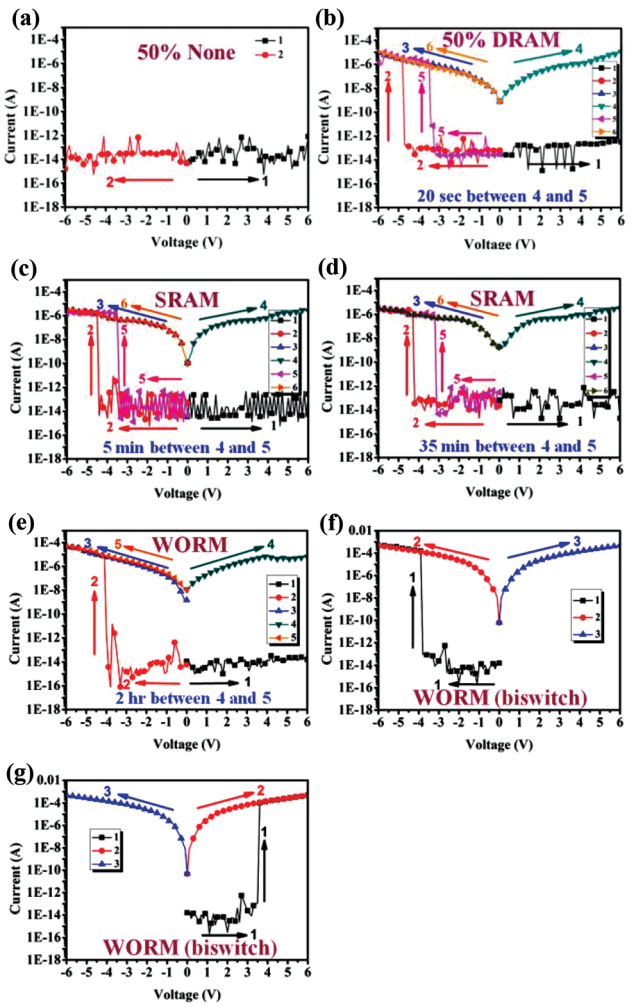

Fig. 7 Current–voltage (*I–V*) characteristics of the ITO/**4ATA-PI**/TiO_2 hybrid material (50 ± 3 nm)/Al memory device: (a) and (b) **4ATA-PITi5**, (c) **4ATA-PITi7**, (d) **4ATA-PITi10**, (e) **4ATA-PITi15**, and (f) and (g) **4ATA-PITi30**.

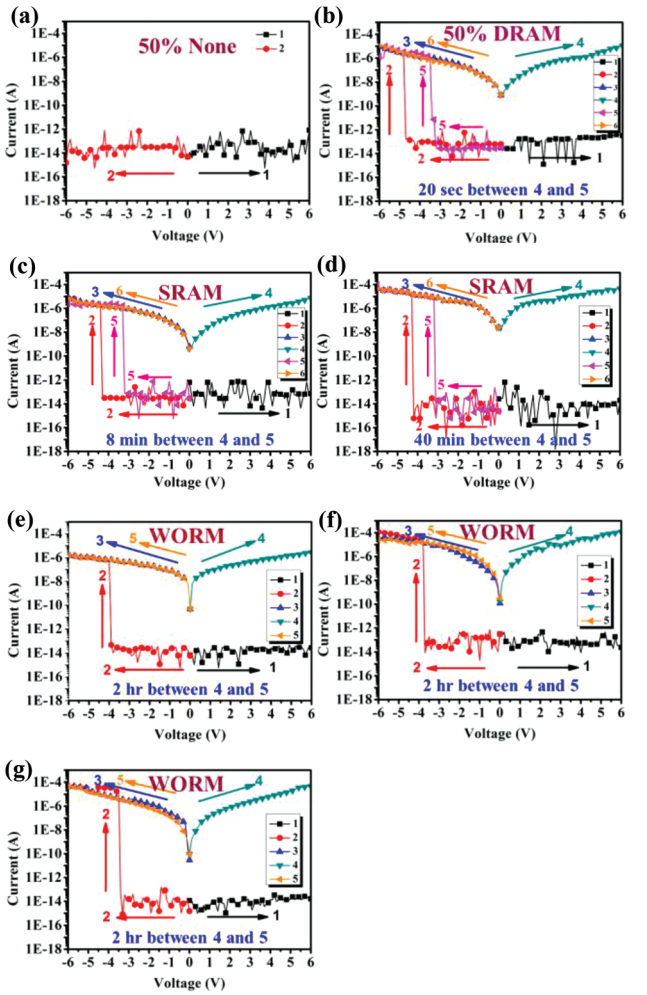

Fig. 8 Current–voltage (*I–V*) characteristics of the ITO/**4ATA-PI**/ZrO_2 hybrid material (50 ± 3 nm)/Al memory device: (a) and (b) **4ATA-PIZr5**, (c) **4ATA-PIZr7**, (d) **4ATA-PIZr10**, (e) **4ATA-PIZr15**, (f) **4ATA-PIZr30**, and (g) **4ATA-PIZr50**.

The memory devices of **4ATA-PITi7** and **4ATA-PITi10** hybrids, containing 7 and 10 wt% of TiO_2, respectively, switched from 10^{-14} to 10^{-5} A at the threshold voltage of −4.4 V (**4ATA-PITi7**) and −4.3 V (**4ATA-PITi10**) in the negative sweep, and the ON state could be read by the subsequent negative (the third sweep) and positive (the fourth sweep) scans as shown in Fig. 7c and d. The ON state would return to the OFF state in 5 min (**4ATA-PITi7**) and 35 min (**4ATA-PITi10**) after removing the applied voltage, and could subsequently switch to the ON state again at the threshold voltage of −3.4 V (**4ATA-PITi7**) and −3.0 V (**4ATA-PITi10**), respectively, implying a volatile SRAM-like behaviour. Comparing to volatile DRAM and SRAM behaviour, the ON state of **4ATA-PITi15** with 15 wt% of TiO_2 could be retained even after turning off the power for 2 h or a longer time since it has been switched on. Thus, the *I–V*

This journal is © The Royal Society of Chemistry 2016

curves of the memory device based on the **4ATA-PITi15** film in Fig. 7e reveal non-volatile write-once-read-many times (WORM) memory properties. Moreover, the devices derived from the **4ATA-PITi30** hybrids containing TiO_2 up to 30 wt% could also be switched to the ON state by a positive voltage of 3.8 V. Thus, the memory devices based on the **4ATA-PITi30** films shown in Fig. 7f and g exhibited bi-switchable characteristics due to the smaller energy gap between the work function of ITO and the LUMO of TiO_2 as shown in Fig. 9b. The stability of the WORM memory devices derived from the **4ATA-PITi30** films both in the ON and OFF states is depicted in Fig. S10 (ESI†).

Furthermore, the memory devices of the **4ATA-PI/ZrO_2** hybrids have also been prepared for comparison, and showed a similar memory behavior to those of the **4ATA-PI/TiO_2** hybrids as shown in Fig. 8. The memory devices of the **4ATA-PIZr5** hybrids with 5 wt% ZrO_2 also have 50% non-memory and 50% DRAM characteristics as shown in Fig. 8a and b, respectively. The threshold voltage is −4.7 V in the negative sweep, and the retention time for returning the ON state to the OFF state is 15 s. The memory device could subsequently switch to the ON state again at the threshold voltage of −3.9 V. Thus, the device behaves with a short retention time and re-writable property which are indicative of DRAM characteristics.

The devices obtained from the **4ATA-PIZr7** and **4ATA-PIZr10** hybrids containing 7 and 10 wt% ZrO_2, respectively, reveal volatile SRAM behavior as shown in Fig. 8c and d. The threshold voltage was around −4.1 V in the negative sweep with a retention time of about 8 min (**4ATA-PIZr7**) and 40 min (**4ATA-PIZr10**). The memory device could subsequently switch to the ON state again at the threshold voltage of around −3.1 V. Interestingly, the **4ATA-PI/ZrO_2** hybrids containing a higher ZrO_2 content up to 50 wt% only revealed non-volatile WORM memory properties depicted in Fig. 8f and g but did not show a bi-switchable behaviour as the result of the corresponding **4ATA-PITi30**, which could be ascribed to the higher LUMO energy level of ZrO_2 than that of TiO_2, and not matching to the ITO work function as shown in Fig. 9c. By introducing TiO_2 and ZrO_2 as electron acceptors into the **4ATA-PI** system, the obtained PI hybrid materials have a lower LUMO energy level that could facilitate and stabilize the charge transfer complex. Therefore, the resulting hybrid memory devices exhibited a high ON/OFF ratio (10^8) with tunable memory properties from DRAM, SRAM, to WORM at a different TiO_2 or ZrO_2 content ranging from 0 wt% to 50 wt% as summarized in Table 5. Generally, the memory device revealed a longer retention time and lower threshold voltage with an increasing inorganic content. In addition, the different LUMO energy level between TiO_2 and ZrO_2 exhibited specifically peculiar memory behaviour in terms of bi-switchable characteristics. Thus, these results obtained in this study suggest the potential application of the prepared **4ATA-PI/TiO_2** and **4ATA-PI/ZrO_2** hybrid films in highly transparent memory devices.

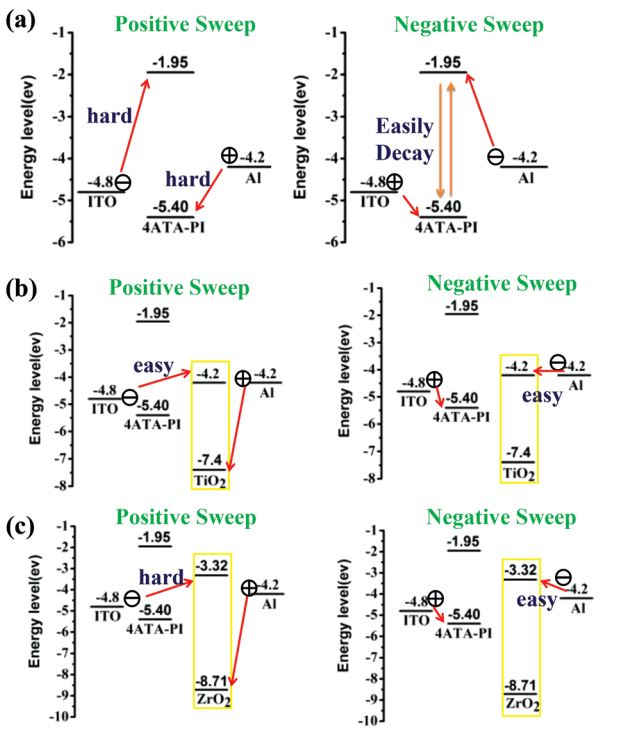

Fig. 9 HOMO and LUMO energy levels of (a) **4ATA-PI**, (b) **4ATA-PI** and **TiO_2**, and (c) **4ATA-PI** and **ZrO_2** along with the work function of the electrodes.

Conclusions

The colorless, transparent, and organo-soluble polyimide (**4ATA-PI**) could be readily prepared by the bio-based alicyclic diamine, 4ATA, and alicyclic dianhydride (BCDA). The carboxylic acid groups in the backbone of **4ATA-PI** provided reaction sites for organic–inorganic bonding, resulting in homogeneous organic–inorganic hybrid films. These PI hybrid films revealed a tunable refractive index (1.60–1.81 for **4ATA-PITi50**, and 1.60–1.80 for **4ATA-PIZr50**). In addition, the optical transparency and Abbe number of the **4ATA-PI/ZrO_2**

Table 5 Summary of **4ATA-PI**, **4ATA-PI/TiO_2**, and **4ATA-PI/ZrO_2** memory properties

4ATA-PI + TiO_2/ZrO_2	0 wt%	5 wt%	7 wt%	10 wt%	15 wt%	30 wt%	50 wt%
TiO_2 memory properties	None	50% none 50% DRAM (15 s)	SRAM (5 min)	SRAM (35 min)	WORM	WORM (bi-switch)	WORM (bi-switch)
ZrO_2 memory properties	None	50% none 50% DRAM (20 s)	SRAM (8 min)	SRAM (40 min)	WORM	WORM	WORM

hybrids are higher than those of the **4ATA-PI/TiO_2** hybrids due to a larger band gap of ZrO_2, implying higher value for optical applications. In addition, by introducing TiO_2 and ZrO_2 as electron acceptors into the **4ATA-PI** system, the obtained PI hybrids have a lower LUMO energy level that could effectively facilitate and stabilize the charge transfer complex. Therefore, these hybrid memory devices exhibited tunable memory properties from DRAM, SRAM, to WORM at a different TiO_2 or ZrO_2 content from 0 wt% to 50 wt% with a high ON/OFF ratio (10^8). The different LUMO energy levels between TiO_2 and ZrO_2 resulted in different WORM-type memory devices (bi-switchable WORM of **4ATA-PITi30** and WORM of **4ATA-PIZr30**).

Acknowledgements

We gratefully acknowledge the financial support for this research through the National Science Council of Taiwan and a partial support through Advanced Low Carbon Technology Research and Development Program (JST, ALCA, 5100270), Tokyo, Japan.

Notes and references

1 T. Nakamura, H. Fujii, N. Juni and N. Tsutsumi, *Opt. Rev.*, 2006, **13**, 104.
2 D. W. Mosley, K. Auld, D. Conner, J. Gregory, X. Q. Liu, A. Pedicini, D. Thorsen, M. Wills, G. Khanarian and E. S. Simon, *Proc. SPIE*, 2008, **6910**, 691017.
3 K. C. Krogman, T. Druffel and M. K. Sunkara, *Nanotechnology*, 2005, **16**, S338.
4 (*a*) L. L. Beecroft and C. K. Ober, *Chem. Mater.*, 1997, **9**, 1302; (*b*) C. Sanchez, F. Ribot and B. Lebeau, *J. Mater. Chem.*, 1999, **9**, 35; (*c*) G. Schottner, *Chem. Mater.*, 2001, **13**, 3422; (*d*) J. Pyun and K. Matyjaszewski, *Chem. Mater.*, 2001, **13**, 3436; (*e*) H. Schmidt, *Appl. Organomet. Chem.*, 2001, **15**, 331.
5 D. W. Mosley, K. Auld, D. Conner, J. Gregory, X. Q. Liu, A. Pedicini, D. Thorsen, M. Wills, G. Khanarian and E. S. Simon, *Proc. SPIE*, 2008, **6910**, 691017.
6 C. A. Terraza, J. G. Liu, Y. Nakamura, Y. Shibasaki, S. Ando and M. Ueda, *J. Polym. Sci. Part A: Polym. Chem.*, 2008, **46**, 1510.
7 (*a*) M. Vert, *Biomacromolecules*, 2005, **6**, 538; (*b*) K. Okano, A. Kondo and H. Noda, *Eco Ind.*, 2006, **11**, 43; (*c*) I. Taniguchi and Y. Kimura, *Biopolymers*, 2001, **3b**, 431.
8 (*a*) M. C. Choi, J. Wakita, C. S. Ha and S. Ando, *Macromolecules*, 2009, **42**, 5112; (*b*) I. A. Ronava and M. Bruma, *Struct. Chem.*, 2010, **21**, 1013.
9 (*a*) T. Matsumoto and T. Kurosaki, *Macromolecules*, 1995, **28**, 5684; (*b*) T. Matsumoto and T. Kurosaki, *React. Funct. Polym.*, 1996, **30**, 55; (*c*) T. Matsumoto, *High Perform. Polym.*, 1999, **11**, 367; (*d*) T. Matsumoto, *Macromolecules*, 1999, **32**, 4933; (*e*) T. Matsumoto, *High Perform. Polym.*, 2001, **13**, 85; (*f*) T. Matsumoto, S. Kawabata and R. Takahashi, *High Perform. Polym.*, 2006, **18**, 719.
10 (*a*) W. Volksen, H. J. Cha, M. I. Sanchez and D. Y. Yoon, *React. Funct. Polym.*, 1996, **30**, 61; (*b*) X. Z. Fang, Z. H. Yang, S. B. Zhang, L. X. Gao and M. X. Ding, *Polymer*, 2004, **45**, 2539; (*c*) M. Hasegawa, M. Horiuchi and Y. Wada, *High Perform. Polym.*, 2007, **19**, 175; (*d*) S. V. Kumar, H. C. Yu, J. Choi, K. Kudo, Y. H. Jang and C. M. Chung, *J. Polym. Res.*, 2011, **18**, 1111.
11 (*a*) T. T. Suzuki, *Macromol. Mater. Eng.*, 2008, **293**, 109; (*b*) M. M. Demir, M. Memesa, P. Castignolles and G. Wegner, *Macromol. Rapid Commun.*, 2006, **27**, 763; (*c*) H. Cui, M. Zayat, P. G. Parejo and D. Levy, *Adv. Mater.*, 2008, **20**, 65.
12 (*a*) G. S. Liou, P. H. Lin, H. J. Yen, Y. Y. Yu, T.-W. Tsai and W. C. Chen, *J. Mater. Chem.*, 2010, **20**, 531; (*b*) C. L. Tsai, H. J. Yen, W. C. Chen and G. S. Liou, *J. Mater. Chem.*, 2012, **22**, 17236; (*c*) H. J. Yen, C. L. Tsai, P. H. Wang, J. J. Lin and G. S. Liou, *RSC Adv.*, 2013, **3**, 17048; (*d*) C. L. Tsai, C. J. Chen, P. H. Wang, J. J. Lin and G. S. Liou, *Polym. Chem.*, 2013, **4**, 4570; (*e*) C. L. Tsai and G. S. Liou, *Chem. Commun.*, 2015, **51**, 13523; (*f*) C. J. Chen, C. L. Tsai and G. S. Liou, *J. Mater. Chem.*, 2014, **2**, 2842.
13 (*a*) H. W. Su and W. C. Chen, *J. Mater. Chem.*, 2008, **18**, 1139; (*b*) R. Himmelhuber, P. Gangopadhyay, R. A. Norwood, D. A. Loy and N. Peyghambarian, *Opt. Mater. Express*, 2011, **1**, 252.
14 H. Althues, J. Henle and S. Kaskel, *Chem. Soc. Rev.*, 2007, **36**, 1454.
15 (*a*) J. Ouyang, C. W. Chu, C. R. Szmanda, L. Ma and Y. Yang, *Nat. Mater.*, 2004, **3**, 918; (*b*) C. W. Chu, J. Ouyang, J. H. Tseng and Y. Yang, *Adv. Mater.*, 2005, **17**, 1440.
16 (*a*) F. Li, T. W. Kim, W. Dong and Y. H. Kim, *Appl. Phys. Lett.*, 2008, **92**, 011906; (*b*) F. Li, D. I. Son, S. M. Seo, H. M. Cha, H. J. Kim, B. J. Kim, J. H. Jung and T. W. Kim, *Appl. Phys. Lett.*, 2007, **91**, 122111.
17 P. Suvannasara, S. Tateyama, A. Miyasato, K. Matsumura, T. Shimoda, T. Ito, Y. Yamagata, T. Fujita, N. Takaya and T. Kaneko, *Macromolecules*, 2014, **47**, 1586.
18 C. J. Chen, Y. C. Hu and G. S. Liou, *Polym. Chem.*, 2013, **4**, 4162.
19 Q. D. Ling, F. C. Chang, Y. Song, C. X. Zhu, D. J. Liaw, D. S. H. Chan, E. T. Kang and K. G. Neoh, *J. Am. Chem. Soc.*, 2006, **128**, 8732.

 This journal is © The Royal Society of Chemistry 2016